Arrospide Eneko (Orcid ID: 0000-0001-7409-6760)

Polymers beyond standard optical fibres – fabrication of microstructured polymer optical fibres

Eneko Arrospide*[a], Gaizka Durana[b], Mikel Azkune[b], Gotzon Aldabaldetreku[b], Iñaki Bikandi[b], Leire Kuiz-Rubio[c], Joseba Zubia[b]

[a] Department of Applied Mathematics, University of the Basque Country (UPV/EHU), Bilbao, Spain.
[b] Department of Communications Engineering, University of the Basque Country (UPV/EHU), Bilbao, Spain.
[c] Chemistry Research Group (LABQUIMAC), Department of Physical Chemistry, University of the Basque Country (UPV/EHU), Leioa, Spain.

***Abstract*— This paper reports the overall fabrication process of microstructured polymer optical fibres (mPOFs). The mPOF fabrication involves a two-step process: on the one hand, the design and creation of a preform containing a large-scale version of the desired fibre and, on the other, the precise heating and drawing of the preform to the final fibre. The preforms are produced either by a improved drilling technique or by capillary stacking. For a correct and accurate drawing of the fibre, a controlled and precise heating unit has to be designed, an issue that will be explained in detail in this work. The quality and optical performance of the final mPOF depends strongly on key factors such as the preform annealing, the accuracy of the technique selected for the creation of the preform**

This article has been accepted for publication and undergone full peer review but has not been through the copyediting, typesetting, pagination and proofreading process which may lead to differences between this version and the Version of Record. Please cite this article as doi: 10.1002/pi.5602

structure, the heating stage, as well as on the drawing parameters. All of them are analysed in detail and some drawn mPOFs of interest are reported as well.

***Index Terms*—Microstructured polymer optical fibre, fabrication, drilling, heat-transfer, fibre drawing.**

INTRODUCTION

Historically, silica dioxide has been the predominant base material for optical fibres. Nevertheless, several constraints have caused the research and development of polymeric fibres mainly using poly(methyl methacrylate) (PMMA). Optical fibres fabricated with other polymers like polycarbonate (PC), polystyrene (PS), or TOPAS have also been reported[1-4]. There is a broad range of applications where polymer optical fibres appear as excellent candidates, such as short range telecommunication networks, biosensing, structural health monitoring, or optical amplification, to name a few[5].

Microstructured polymer optical fibres (mPOFs) were first demonstrated in 2001[6], based on previous designs for silica photonic crystal fibres (PCF), and since then a large variety of microstructure designs have been considered for mPOFs[7-11]. The combination of polymer and microstructure has allowed the achievement of many purposes and optical properties for the first time, such as single-mode guidance in polymer fibres in the visible[6], or hollow core (HC) mPOFs, where light is guided through the air-filled core, which has a lower refractive index than the surrounding material[12].

In this work, we analyse the overall fabrication process of mPOFs, focusing on the mechanical and chemical properties of the polymers employed, mainly PMMA. In comparison with the well known silica photonic crystal fibres fabrication process, the use of polymers requires specific treatment, such as one

* Correspondence to: Eneko Arrospide, Department of Applied Mathematics, University of the Basque Country (UPV/EHU), Plaza Ingeniero Torres Quevedo 1, 48013, Bilbao, Spain. E-mail: eneko.arrospide@ehu.eus

annealing stage prior to the preform fabrication process, or the development of ad-hoc drilling and capillary stacking techniques, depending on the mechanical properties of the polymer. In addition, during the drawing stage, a complete thermodynamic analysis must be performed, due to the lower glass transition temperature (T_g) values of the polymers compared to silica, so that the heating units of the drawing tower must be specifically designed and fixed[13].

Material properties of PMMA are detailed first, with special interest on the optical, mechanical and chemical properties. This way, critical parameters like T_g or weight-average molar mass (M_w) are analysed. In the preform creation stage, fabrication techniques are described, namely drilling and capillary stacking. Softness of the polymers makes necessary the use of improved drilling bits. The automatization of the drilling technique requires the use of a high precision Computer Numerical Control (CNC) machining centre, in which drilling parameters must be specifically fixed. Regarding the capillary stacking technique, constraints such as static electrical charge of the polymer capillaries and rods must be solved. Afterwards, the fibre drawing stage is explained in detail. The drawing tower must be specifically designed considering the properties of the polymers that will be drawn to fibre, designing the most suitable heating and stretching units. Finally, some mPOFs fabricated in our fibre drawing tower are analysed and the main conclusions are summarized.

MATERIALS

There are some fundamental requirements that should be fulfilled by materials aimed at enhancing mPOF performance[11,14]. As explained in a later section, the fabrication of mPOFs relies on fibre drawing, which is a physical process where a softened polymer flows smoothly when it is pulled down. Thermoplastics are

good candidates since they flow at high temperatures. However, not all thermoplastics are adequate for drawing optical fibres. Their molecular weight is also an important parameter that must be taken into account when selecting a polymer. Additionally, high transparency in the visible region of the electromagnetic spectrum and mechanical flexibility are also fundamental requirements to consider when choosing a fibre material. At present, mPOFs are mainly fabricated using PMMA or TOPAS. The latter presents the advantage of lower moisture absorption and is highly transparent in the THz regime. However, because PMMA is relatively cheap, widely available, and has low attenuation in the visible, from now on we will focus on this material.

Using the Differential Scanning Calorimetry technique and the Gel Permeation Chromatography technique, T_g and M_w of commercially available PMMA rods[15] have been measured, respectively. Results are shown in Figure 1. The data points concentrated in the lower left corner of the graph (cross markers) correspond to extruded PMMA, whereas data points in the upper right corner have been obtained for cast PMMA. In the latter case the polymer chains are too large and the polymer does not flow even at high temperatures above T_g. The polymer shows a rubbery behaviour and the required temperature to draw the preform exceeds the degradation temperature of the polymer. Low values of M_w are neither desirable because PMMA preforms have a very narrow glass transition range that makes it difficult to find good drawing conditions. In contrast, data from extruded PMMA shown in Figure 1 (cross markers) fall somewhere in between both cases and meet the adequate conditions for good drawing.

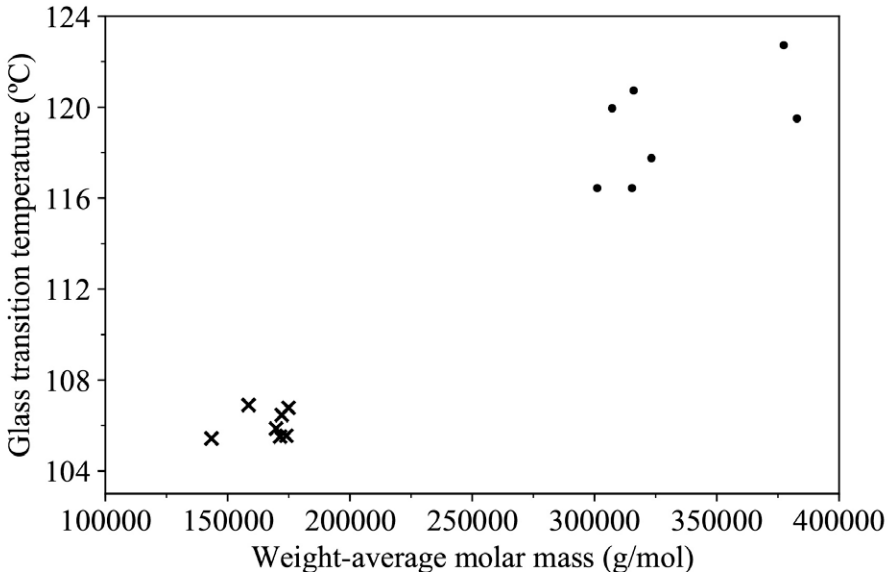

Figure 1. Distribution of glass transition temperatures T_g against weight-average molar mass M_w of several commercially available PMMA preforms obtained by extrusion (cross markers) and casting (circle markers).

A correct thermal treatment of the rods is fundamental to avoid undesirable effects in the preform. Figure 2 shows an example of a preform that foamed during drawing as a result of an incorrect preparation. Most bubbling is concentrated in the neck-down region where the temperature is the highest. Most probably, this is the result of unreacted monomer particles, rest of initiators, solvent residues or simply diffused moisture into the preform[16]. These problems arose during the fabrication tests carried out in our drawing tower. Due to the high water absorption capacity of PMMA, it is necessary to anneal the preforms in order to avoid the appearance of air bubbles during drawing. The annealing process consists in the removal of all moisture from the preforms, keeping them in a low humidity and high temperature atmosphere, below T_g, for long periods of time. In our case, the preforms where annealed for 14 days at 90 ºC in a climate chamber.

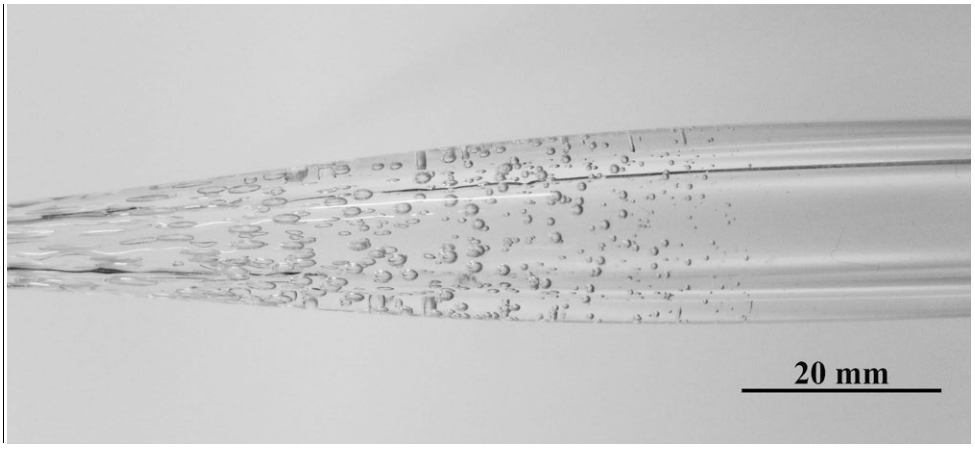

Figure 2. Preform (20 mm in diameter) bubbling during drawing as a consequence of a small amount of volatile particles present in the preform.

PREFORM CREATION

In the first stage of the mPOF fabrication process, a macroscopic polymer preform is fabricated, which contains a large scale version of the desired microstructure in the fibre. Different techniques can be employed in the preform fabrication process. Among the different fabrication methods available[8], in this work we focus on drilling and capillary stacking.

Regarding the drilling method, our CNC machining centre offers an easy way to obtain different and accurate geometries for preform structures. On the other hand, the capillary stacking technique provides the capacity to create preforms with very high air proportion, being such structures almost impossible to obtain by drilling.

Drilling

Drilling is the most widely used technique for the fabrication of polymer preforms. Using a CNC machining centre it is possible to execute a sequence of automatized instructions over a monolithic polymer cylinder fixed in the workholder, in order to fabricate complex structured preforms with high precision.

CNC machining centres offer an easy way to obtain different geometries for preform structures by changing the diameters of the holes, the spacing of the holes, and their distribution in the polymer (see Figure 3). Taking into account that polymer is a soft material in general, all parameters that characterize the drilling process (cutting-speed, spindle-speed, feed, depth of cut, etc.) are completely different from those used to drill materials like glass, steel or iron. Therefore, and depending on the kind of polymer, it is necessary to fix these parameters accurately in order to avoid problems such as roughness in the surface of the holes or melting in the polymer due to high temperatures during the drilling.

The use of the drilling method in the fabrication of the polymer preform imposes a limitation in the maximum length of the preform. Even with deep hole drilling bits, relatively short preforms can only be processed. So far, preforms of about 70 mm in length have been reported with holes of 2 mm in diameter[17].

In our experience, drilling the solid preform using high-speed steel twist drill bits generates long chips that melt and jam the holes. For this reason, it is necessary to lift the drill bit from the hole repeatedly in order to remove the chips jammed in the helix and cool the hole using external coolant. As a result, this approach makes the preform fabrication an extremely complex and time-consuming process. With the aim of overcoming this limitation, we have improved the drilling technique using through coolant drill bits. The coolant is supplied to the polymer preform through the drill, achieving a more efficient removal of the chip, a continuous cooling of the drilled position of the preform and an increase in the depth of cuts. Moreover, as employing these kinds of drill bits provides an improvement in the quality of the drilled holes and a significant reduction in the time required for the drilling. Figure 3 shows a preform fabricated using through coolant drill bits.

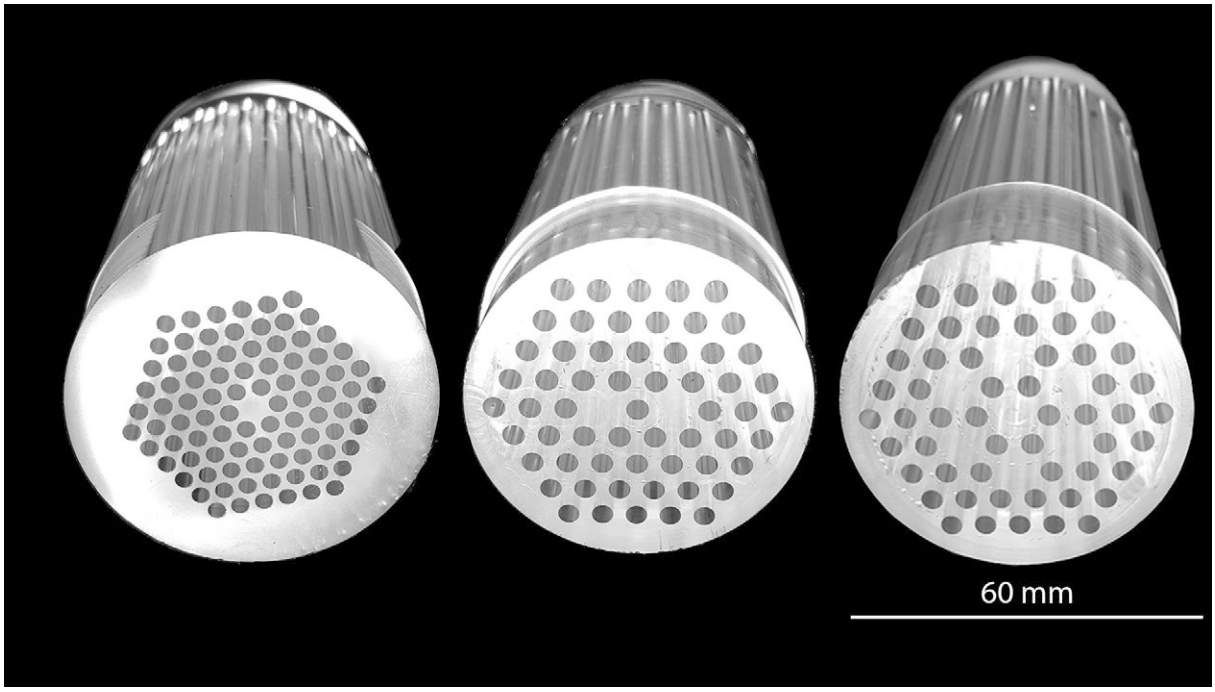

Figure 3. Three solid core preforms (60 mm in diameter) created by drilling, using bits of 3 mm.

Capillary stacking

This preform creation method is a handmade process that, on the one hand makes the method more laborious and complex, but, on the other hand, enables the fabrication of some complex preforms that are not possible to obtain by using the drilling method. Thus, preforms with very high air proportion can be fabricated, like Kagome lattice preforms[18], and the limitation in the preform length imposed by the drilling method is overcome.

In this method, capillaries and tubes are placed one row at a time, using an ad-hoc designed jig (see Figure 4 (a)). Once the stack is complete, the last step in the creation of the preform consists in the accurate sleeving of the stack into a tube (see Figure 4 (c)), together with the insertion of fixing tubes in the stack (see Figure 4 (b)), in order to avoid deformations in the desired structure. Notice that during the process,

the small diameter rods and the thin wall capillaries become electrically charged. Static electricity can seriously hinder the stacking process (see Figure 4 (d)), and therefore, in order to remove it, a high voltage electric field applied to the capillaries creates a stream of ions that neutralizes the static charge stored in the capillaries and rods. Figure 4 (e) shows a preform created by capillary stacking, in which only capillaries have been employed.

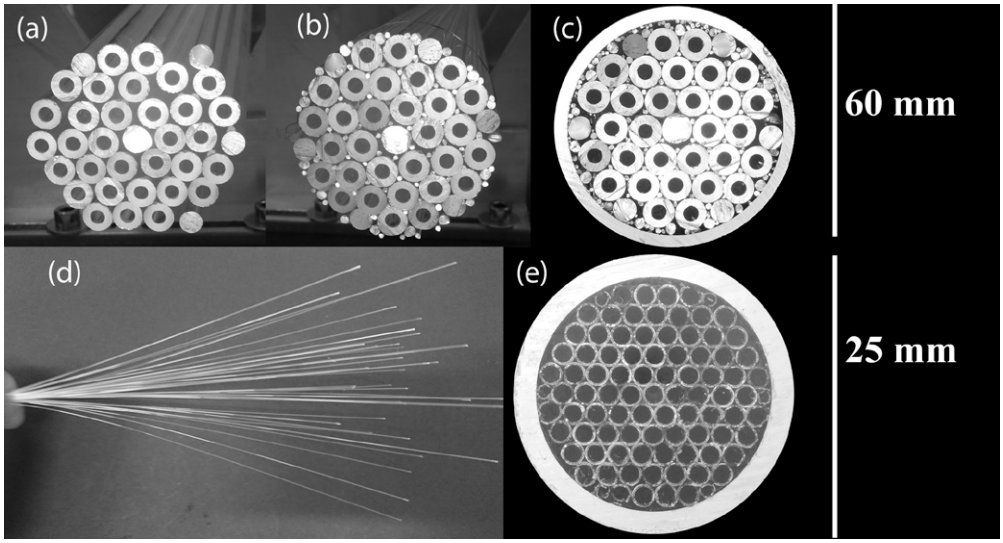

Figure 4. (a-c) Steps in the creation of a preform by capillary stacking, using capillaries and rods of different diameters sleeved into a 60/54 mm tube, (d) electrically charged capillaries repelling each other, and (e) a final preform created by stacking together capillaries sleeved with a tube of 25/21 mm in diameter.

DRAWING TO FIBRE

Description of the general drawing process

Figure 5 shows the scheme of a typical drawing tower. The drawing process is in essence the same as that followed with conventional fibres: during the heating process of the preform in the furnace, a stepper motor

is responsible for feeding it into the furnace at an adequate rate to ensure that the preform temperature will rise above T_g in order to have the polymer ready for stretching.

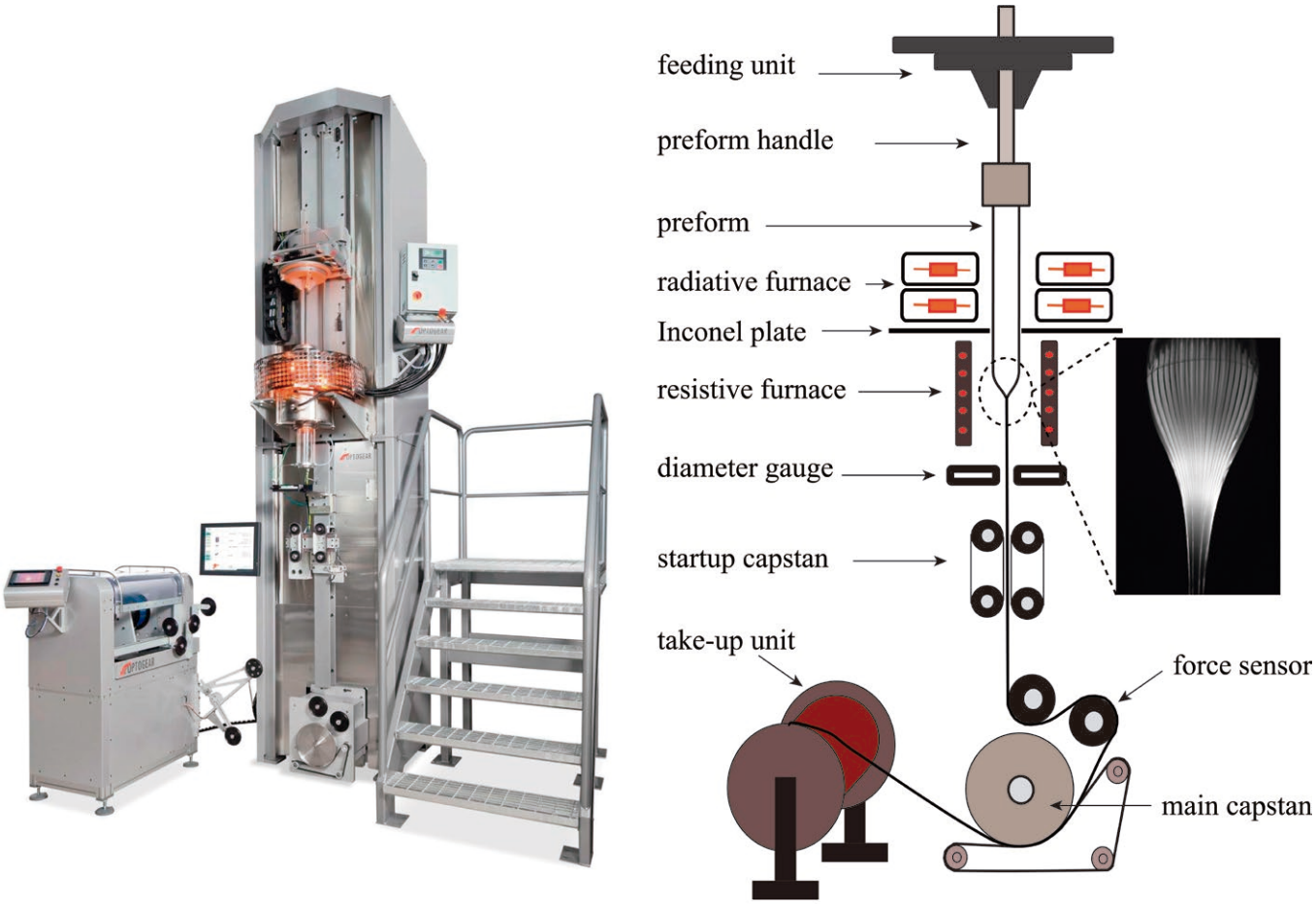

Figure 5. Photograph and schematic diagram of the drawing tower. The close-up picture shows the neck down region of an mPOF preform.

When the heated preform is pulled down at a higher speed, namely draw speed (v_{draw}), the so-called neck-down region is created. This region refers to the preform section starting at the hottest point where a rapid change in the preform diameter occurs (see Figure 5). The shape and length of the neck-down region is of primary importance when manufacturing mPOFs because of its impact on the hole deformation and on

the diameter control. Under steady conditions, mass conservation dictates the final diameter (D_f) as a function of preform feed rate (v_{feed}), preform diameter (D_0) and draw speed (v_{draw})[8]:

$$D_f = D_0\sqrt{\frac{v_{feed}}{v_{draw}}}, \quad (1)$$

where the draw speed is determined from the speed of a point on the rotating circumference of the main capstan, and the final diameter is measured during the drawing using a laser-based system that records the diameter in two perpendicular directions. The drawing force is also measured by means of a force sensor installed in one of the pulleys of the main capstan (see Figure 5).

Furnace design: heating process

During preform drawing, a key factor for minimizing deformation of the microstructure is the uniformity of the temperature profile in the cross section of the preform. Although heating polymer preforms is conceptually similar to the case of glass preforms, in practice the situation is quite different because of the differing material properties and preform characteristics. First of all, thermal conductivity of the polymers used for mPOF fabrication is poor (one order of magnitude lower in the case of PMMA). In addition to that, preform size is much larger in the case of mPOFs: preforms for glass PCFs are typically several centimeters in diameter (2-3 cm), whereas primary preforms for mPOF fabrication are 6-8 cm in diameter. An extra difficulty when drawing structured polymer preforms lies in the presence of a large air fraction within the structure that requires considering the interplay between conduction and radiation modes of heat transfer within the preform[19]. Therefore, since the exact furnace design and operation profoundly affects the quality and extent of the hole deformation[17], the optimal heating conditions for each preform design are to be determined empirically by trial and error, for each drawing tower, even though it is still possible to provide general guidelines valid for any drawing tower.

The overall furnace consists of two sections: an air-cooled radiative furnace used as preheat section, and a resistive furnace for drawing the preform (drawing section). The radiation furnace contains six infrared lamps arranged at two different heights. At each height three lamps form an equilateral triangle, and both lamp triangles arranged in this way are rotated 60º with respect to each other. A glass cylinder placed inside the triangles provides preform protection against the stream of air used to cool the lamps. Regarding the resistive furnace, a stainless steel tube wound with heating wires acts as the oven. Due to the large size of the preforms, the drawing process is mainly done following a two-stage process; for the preform-to-cane stretching, a large diameter steel tube is required, whereas cane-to-fibre drawing is performed with a small diameter steel tube. Optionally, an Inconel plate separates both sections of the furnace. In addition, two irises isolate each section from the outer atmosphere.

Furnace design: preheating

The preheating section is aimed at raising the preform temperature to around 110 ºC to ensure that the preform will enter the drawing section without any deformation. The challenge comes primarily from the need to get a uniform heating in the cross section of the large preform (in our case, primary preforms of 6 cm in diameter).

Among the different heating strategies considered, we have obtained the best results with the step-like furnace temperature scheme. A solid PMMA preform (preform diameter: $\phi_{preform}$= 60 mm) was used for that purpose. Five K-type thermocouples were located at five radial positions, and their axial position was the same: 45 mm from the top of the preform. The measured temperatures as a function of time are plotted in Figure 6.

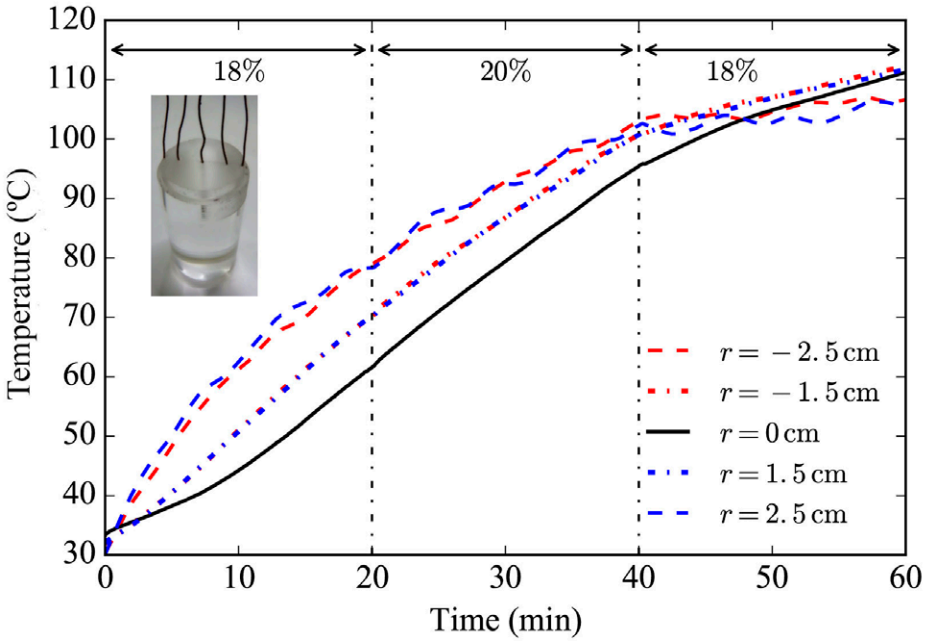

Figure 6. Evolution of temperature at five different radial points (r= -2.5, -1.5, 0, 1.5, and 2.5 mm) of a 100 mm long solid PMMA preform of 60 mm in diameter. Each time slot of 20 min is associated to a power level of the radiative furnace that follows a step-like profile: 18% from 0 to 20 min; 20% from 20 to 40 min; 18% from 40 to 60 min. The power expressed as a percentage refers to the maximum power level delivered by the radiative furnace.

First of all, it is noteworthy the azimuthal symmetry of the preform heating. The temperature of the diametrically opposed points ramp up together. Regarding the time evolution of the radial distribution of the preform temperature, the underlying physical process may be understood in the following way: at early stages, the preform surface heats fast. The poor thermal conductivity of the polymer turns into a time lag before the central region of the preform feels the effects of the surface heating. For this reason the surface temperature further increases during the early stages (first half of the step-up furnace temperature: 0-20 min; furnace power set at 18 % of its maximum value). After finishing the step-up heating (second half of

the step-up, min 20 to min 40; furnace power set at 20 %), the furnace power is decreased back to its initial value of 18 % to prevent the surface from overheating and to allow the preform centre to progress and even surpass the surface temperature. If we define the radial uniformity of the temperature profile as

$$\Delta T = \left(\frac{T_{max} - T_c}{T_c}\right) \times 100, \quad (2)$$

where T_{max} refers to the maximum preform temperature at a given time, and T_c to the temperature of the preform centre at the same time, the maximum uniformity is achieved almost at the end of the step-down stage (see Figure 7). A unique step-up heating scheme of the radiative furnace is also shown in Figure 7 (solid line). The results clearly show that the step-up step-down scheme is preferable in terms of radial uniformity of the temperature. As it can be observed, the difference of temperature between any two points of the preform is lower than 2 %.

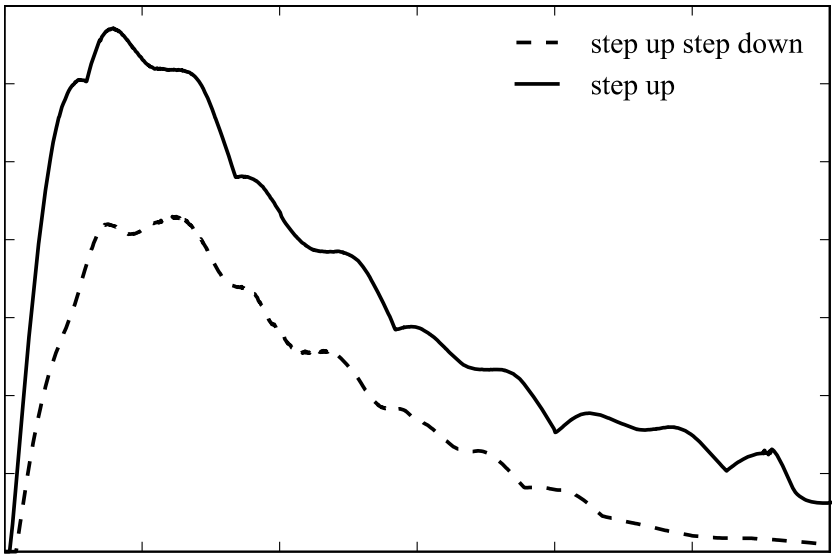

Figure 7. Evolution of temperature difference ΔT between the centre and the hottest measured point of a solid PMMA preform for two different heating schemes.

Furnace design: drawing process

After the preform has been preheated, it enters the drawing section. At this stage it is important to point out the relevance of using an Inconel plate to separate both furnace sections in order to guarantee an independent and stable operation of the resistive furnace.

Figure 8 shows the evolution of the temperature in the resistive furnace with and without the Inconel plate. In the former case, the temperature is essentially constant with a standard deviation of only 0.2 ºC. However, in the latter case, the absence of a physical barrier between both sections sets an oscillatory air flow within the drawing section that causes the recorded air temperature to oscillate with a standard deviation of 0.5 ºC. These air temperature oscillations promote an instability mode that has a negative impact on the drawing fibre diameter[13]. Therefore, care must be taken when setting the thermal boundary conditions of the drawing section to guarantee steady operation. In our case, steady operation was achieved separating both preheat and drawing sections using the Inconel plate.

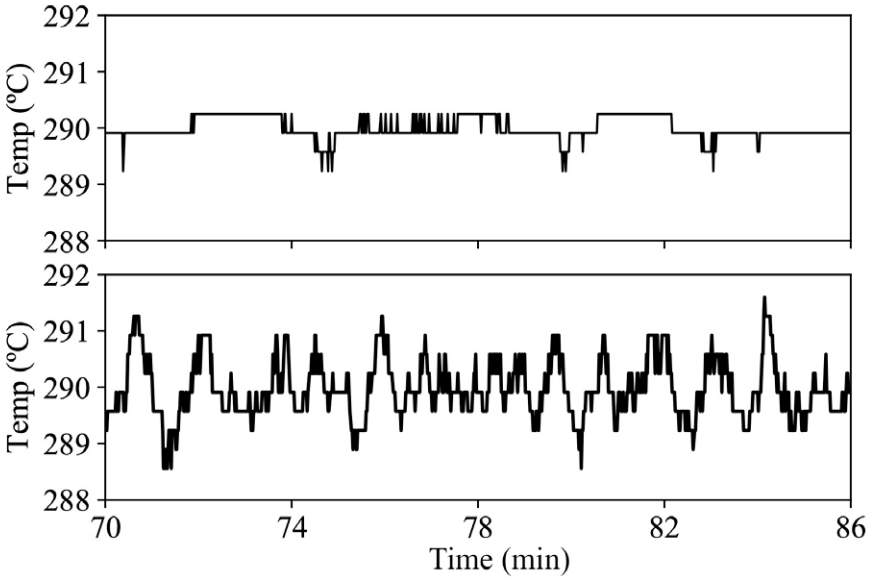

Figure 8. Measured temperature in the drawing section (a) with and (b) without the Inconel plate installed between the preheat and drawing sections.

Drawing preforms

The primary preform, prior to final drawing, follows an intermediate stage where it is stretched to a microstructured cane of around 6 mm in diameter. This two-step procedure ensures a precise control of the fibre diameter, because large drawing ratios would affect negatively to the stability of the fibre diameter (v_{draw}/v_{feed} would be around 3600-90000 if the primary preform were drawn directly to fibre). In some mPOF designs it is also necessary to sleeve the cane with a PMMA or PC tube in order to get the specified hole and core dimensions in the final fibre (in the sleeving process, the microstructured cane is inserted first into a polymeric tube with an inner diameter slightly larger than the diameter of the cane, and then the air gap created in between is connected to a vacuum system in order to fuse the cane and the tube together, yielding the so-called secondary preform). The final step involves drawing the intermediate cane or

secondary preform down to the final fibre. The results obtained at each stage of the drawing process are shown in Figure 9.

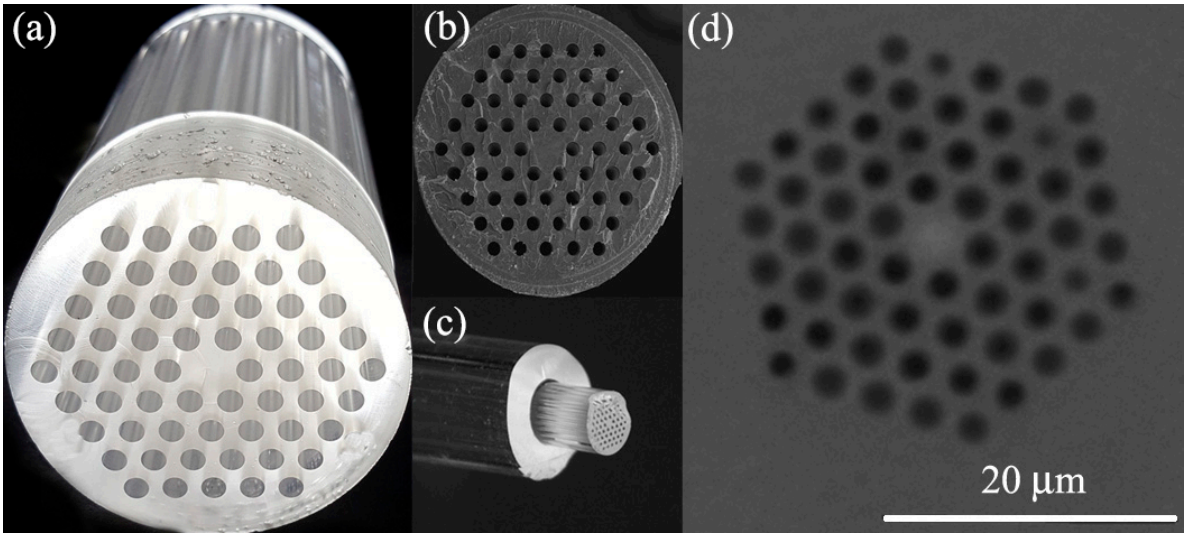

Figure 9. Sequence of steps followed in the drawing process from the (a) primary preform of 60 mm in diameter and 100 mm in length, to (d) the final fibre. (b) Cross section of the intermediate cane of 6 mm in diameter. (c) Secondary preform obtained from the cane sleeved with a PMMA tube of dimensions 12/6 mm (outer/inner wall diameters).

The dominant factors that affect the drawing process are the drawing ratio (v_{draw}/v_{feed}) and the drawing temperature. The latter is aimed at keeping the tension of the drawn fibre under control, typically around 70 g, so that during the drawing process small temperature adjustments may be done in order to ensure a fibre drawing at constant tension. Figure 10 (left) shows the temporal evolution of the diameter of several capillaries used for capillary stacking, whereas Figure 10 (right) shows the variation of the diameter with the length of several fibres drawn in our drawing tower. Note that the diameter remains stable with an standard deviation that, in most cases (Figure 10 (a) to (e)) is well below 1% of the corresponding average value; and in the worst case (Figure 10 (f)) it only accounts for 2% of its average value. Assuming

conservation of mass, and for selected tube or secondary preform diameter, the drawing ratio defines a nominal final diameter through Eq. (1) that –in every case of Figure 10– fits well the measured experimental values. These results are summarized in Table 1.

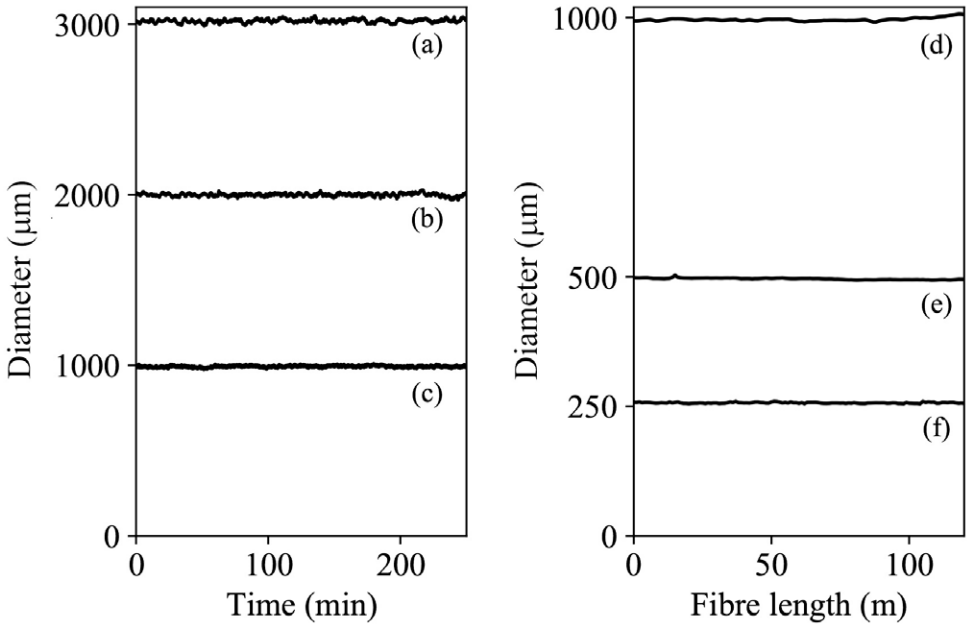

Figure 10. (Left) Outer diameter of several capillaries as a function of time during steady state operation of the drawing process. Average and standard deviation values of outer diameters: (a) (994±6) μm, (b) (1999±9) μm, (c) (3020±10) μm; (right) fibre diameter as a function of its length during steady state operation of the drawing process. Average and standard deviation values of diameters: (d) (1004±7) μm, (e) (499±2) μm, (f) (248±5) μm.

Table 1. Comparison of the experimental diameter with the calculated diameter through Eq. (1) assuming conservation of mass for the case of three different capillaries (first three rows) and three different fibres (last three rows).

Preform diameter (mm)	Feed speed (mm/min)	Draw speed (m/min)	Measured diameter (μm)	Nominal diameter (μm)

20	2	0.089	3020 ± 10	3002
20	2	0.204	1999 ± 9	1979
20	0.5	0.197	994 ± 6	1007
40	0.2	0.320	1004 ± 7	1000
20	0.5	0.829	499 ± 2	491
20	0.5	3.135	248 ± 5	253

EXAMPLES OF mPOFs DRAWN IN OUR FACILITY

The rich variety of new features of mPOFs beyond those that conventional fibres are able to offer, in combination with the advantages of using polymer as manufacturing material, means that the number of applications of mPOFs is widening into ever increasing areas of science and technology. In this section, representative mPOF designs fabricated in our drawing tower are reported, and some of their interesting applications are discussed to underline the advantages of mPOFs over conventional POFs and silica fibres. All these mPOFs were obtained following the general fabrication guidelines described in previous sections.

Single-mode operation for polarimetric and interferometric devices

Although POF technology is dominated by highly multimodal fibres operating in the visible range[5], endlessly single-mode operation is also possible when dealing with mPOFs. Figure 11 illustrates the concept of single-mode guidance of light. The pattern of holes behaves like a sieve. Only the fundamental mode is confined within the fibre core (Figure 11 (a)). Higher order modes escape through the bridges (Figure 11 (b)). If the diameter of the air holes increases, the bridges get narrower and these higher order

modes become trapped in the core. Therefore, the bridge size (or the ratio of hole diameter to hole spacing) defines the modal regime of the mPOF.

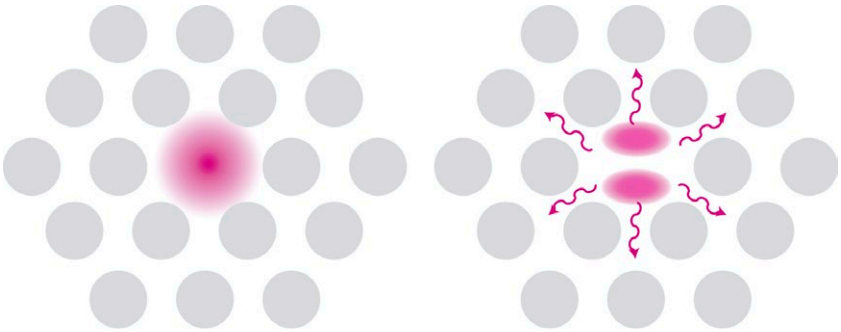

Figure 11. (a) The fundamental mode is well confined by the structure because the mode does not fit within the gaps between the air holes –the mode is spatially too large to pass through the bridges. (b) The higher order mode is able to escape through the bridges because its effective wavelength in the transverse plane is smaller.

Figure 12 (a) shows the primary preform and the cross section of the corresponding single-mode mPOF of four rings of holes drawn from this preform. The drawn fibre is the result of a double sleeving process giving rise to an outer diameter of 250 μm and air holes of 3 μm in diameter. This mPOF provides single-mode guidance in the visible range of the spectrum and it has proved to be a good candidate for the design and development of polarimetric and interferometric devices aimed at sensing purposes[14,20-23].

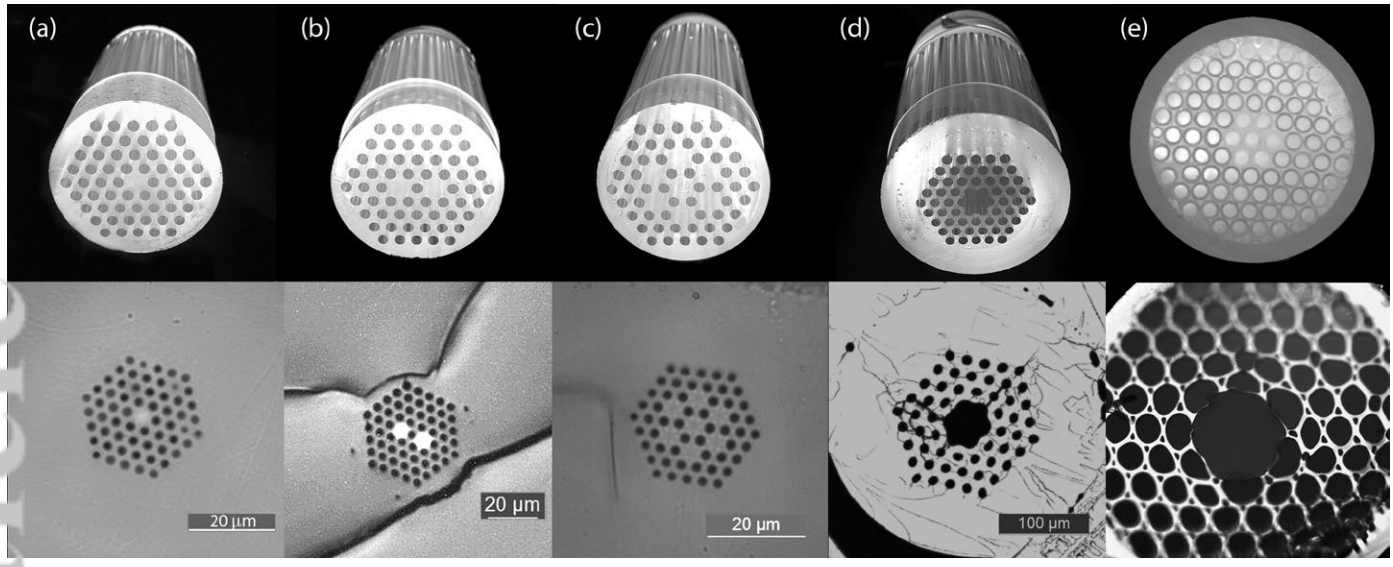

Figure 12. Primary preforms (first row) and their corresponding mPOFs drawn in our drawing tower (second row).

By drilling a slightly different holey structure in the solid PMMA preform, dual-core and seven-core mPOFs have been fabricated (see Figure 12 (b) and (c)). In this type of fibres (multi-core fibres or MCFs), the particular feature that makes them interesting for various optical sensing applications is the interference pattern that builds up from the excitation of several supermodes of the MCF. A short segment of such a MCF constitutes the central element for the construction of MCF-based interferometers that are highly accurate and sensitive to strain sensing[24].

Liquid based sensing

A field where mPOFs are likely to have a major impact is biosensing or, more specifically, optofluidic sensing applications[25-27]. Optical fibres in general – and mPOFs in particular – have the ability to increase the overlap between the guided light and the sensing material. In the case of mPOFs, this is mainly achieved using specific fibre geometries that enable the interaction between light and material. The degree

of overlap depends on whether the material is placed in the core or not; in any case, the holes of the structure have to be filled with the sensing material.

Figure 12 (d) shows the primary preform created by drilling and the corresponding HC mPOF. The preform has been created by drilling a central hole to the classical hexagonal ring pattern (shown in Figure 12 (a)). Similarly, the HC mPOF shown in Figure 12 (e) has been fabricated using capillary stacking. Both HC mPOFs are targeted to maximize the interaction between the guided light and the sensing material by inserting the latter into the core.

CONCLUSIONS

We have reported on a fabrication process in our fabrication facility that can be used to draw a great variety of mPOFs. Although we have applied the fabrication process to technical grade extruded PMMA preforms, it can be easily adapted to other polymers of interest. Key parameters during the fabrication process are, on the one hand, a tight control of the heat transfer within the preform during the preheating and fibre drawing phases and, on the other hand, the tension applied to the fibre during drawing. The flexibility of the fabrication process available for polymers, their mechanical advantages, and the broad scope of development offered by them through the inclusion of nanoparticles, doping and grafting, make mPOFs attractive to cover a range of applications that silica fibres could hardly address.

ACKNOWLEDGMENTS

This work was supported in part by the European Regional Development Fund, in part by the Ministerio de Economía y Competitividad under project TEC2015-638263-C03-1-R, and in part by the Gobierno

Vasco/Eusko Jaurlaritza under projects IT933-16 and ELKARTEK (KK-2016/0030, KK-2017/00033, KK-2017/00089 and KK-2016/0059). The work of Mikel Azkune was supported in part by a research fellowship from the Universidad del Pais Vasco / Euskal Herriko Unibertsitatea (UPV/EHU), Vicerrectorado de Euskera y Formación Continua.

REFERENCES

1 Koike Y and Asai M, *NPG Asia Mat* **1**: 22-28 (2009).

2 Zubia J and Arrue J, *Opt. Fiber Technol* **7**: 101-140 (2002).

3 Emiliyanov G, Hoiby P-E, Pedersen L-H, Bang O, Opt. *Sensors* 2013, *13*(3), 3242-3251

4 Emiliyanov G, Jensen J-B, Bang O, Hoiby P-E, Pedersen L-H, Kjær E-M, and Lindvold L, Opt. Lett. 32, 460-462 (2007)

5 Ziemann O, Krauser J, Zamzow PE and Daum W. POF handbook: optical short range transmission systems. Springer-Verlag Berlin Heidelberg, (2008).

6 Eijkelenborg MA, Large MCJ, Argyros A, Zagari J, Manos S, Issa N, Bassett I, Fleming S, McPhedran R, Sterke CM and Nicorovici NA, *Opt. Express* **9**: 319-327 (2001).

7 Argyros A, *J. Lightwave Technol* **27**: 1571-1579 (2009).

8 Large MCJ, Poladian L, Barton G, Eijkelenborg MA, Microstructured Polymer Optical Fibres. Springer, (2008).

9 Beckers M, Schlüter T, Vad T, Gries T, Bunge C-A, *Polym. Int*. **64**: 25–36 (2015).

10 Ortega B, Min R, Sáez-Rodriguez D, Mi Y, Nielsen K, Bang O. Bandpass transmission filters based on phase shifted fiber Bragg gratings in microstructured polymer optical fibers. In Proceedings of the SPIE, Prague, Czech Republic, id. 1023209 11 pp. (2017).

11 Bunge C-A, Beckers M, Gries T, Polymer Optical Fibres: Fibre Types, Materials, Fabrication, Characterisation and Applications. Woodhead Publishing- Elsevier (2016)

12 Argyros A, Leon-Saval SG, Pla J and Docherty A. *Opt. Express* **16**: 5642-5648 (2008).

13 Reeve HM, Mescher AM and Emery AF. *J. Heat Transfer* **126**: 236-243 (2004).

14 Argyros A, *ISRN Optics*, 785162 (2013).

15 Evonik. https://www.plexiglas-shop.com/pdfs/en/211-12-PLEXIGLAS-Tubes-Rods-en.pdf [accessed 5 October 2017].

16 Kuzyk MG. Polymer Fiber Optics: Materials, Physics, and Applications. CRC Press LLC. (2006).

17 Barton G, Eijkelenborg MA,Henry G, Large MCJ and Zagari J, *Opt Fiber Technol* **10**: 325-335 (2004).

18 Argyros A and Pla J, *Opt. Express* **15**: 7713-7719 (2007).

19 Xue SC, Lwin R, Barton G, Poladian L and Large MCJ, *J. Lightwave Technol* 25: 1177-1183 (2007).

20 Durana G, Arrizabalaga O, Arrospide E, Aldabaldetreku G, Zubia J and Azkune M. *#. Lightwave Technol* **35**: 3035-3041 (2017).

21 Durana G, Gómez J, Aldabaldetreku G, Zubia J, Montero A and Sáez de Ocáriz I, *IEEE Sens. J.* **12**: 2668-2673 (2012).

22 Large MCJ, Blacket D, Bunge CA, *IEEE Sens. J.* **10**:1213-1217 (2010).

23 Saez-Rodriguez D, Cruz JL, Johnson I, Webb DJ, Large MCJ and Argyros A, *IEEE Sens. J.* **10**: 1169-1173 (2010).

24 Villatoro J, Arrizabalaga O, Durana G, de Ocáriz IS, Antonio-Lopez E, Zubia J, Schülzger A and Amezcua-Correa R, *Sci. Rep.* 7: 4451 (2017).

25 Cox FM, Argyros A, Large MCJ and Kalluri S, *Opt. Express* **15**: 13675-13681 (2007).

26 Cox F, Argyros A, Large MCJ, *Opt. Express* **14**: 4135-4140 (2006).

27 Azkune M, Bikandi I, Aldabaldetreku G, Berganza A, Durana G, López A, Zubia J. High reproducibility SERS snsing platform using hollow core microstructured polymer optical fibers. In Proceedings of 24th International Conference on Plastic Optical Fibers, POF 2015, Nuremberg, Germany, p. 227-231 (2015).